LANGMUIR

pubs.acs.org/Langmuir Article

Coexistence and Coevolution of Wrinkle and Ridge Patterns in the Film−Substrate System by Uniaxial Compression

Senjiang Yu,*,‖ Jiahui Zhang,‖ Hong Zhou, Yadong Sun, and Yong Ni*

Cite This: *Langmuir* 2024, 40, 403−412 Read Online

ACCESS | Metrics & More | Article Recommendations | Supporting Information

ABSTRACT: Homogeneous wrinkles and localized patterns are ubiquitous in nature and are useful for a wide range of practical applications. Although various strain-driven surface instability modes have been extensively investigated in the past decades, understanding the coexistence, coevolution, and interaction of wrinkles and localized patterns is still a great challenge. Here, we report on the formation and evolution of coexisting wrinkle and ridge patterns in metal films deposited on poly(dimethylsiloxane) (PDMS) substrates by uniaxial compression. It is found that the evolving surface patterns show unique features of morphological transition from stages I to III: namely, transition from localized ridges to coexisting wrinkles and ridges, and finally to sinusoidal-like structures, as the compression increases. Based on the compressive strain-driven surface instability theory and finite element numerical simulation, the morphological features, transition behaviors, and underlying mechanisms of such complex patterns are investigated in detail, and the changes of amplitude and wavelength versus the strain are consistent with our experiments. This work could promote a better understanding of the effect of strain localization and the interaction of multiple surface patterns in hard film−soft substrate systems.

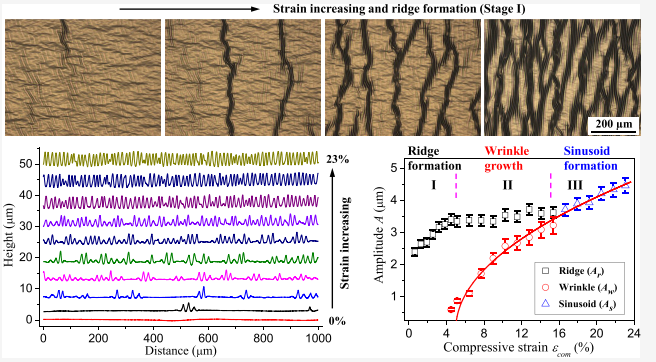

Downloaded via FUDAN UNIV on January 30, 2024 at 03:47:10 (UTC).
See https://pubs.acs.org/sharingguidelines for options on how to legitimately share published articles.

INTRODUCTION

Bowden et al.[1] reported the spontaneous formation of homogeneous and controllable wrinkles in gold films deposited on polydimethylsiloxane (PDMS) substrates when the system was cooling.[1] Thereafter, wrinkle patterns have received a great deal of attention for both fundamental investigations and engineering applications. It is now well-known that wrinkles are typically generated in the bilayer system of a thin rigid film resting on a thick, soft substrate when the imposed compressive stress exceeds a threshold. The mechanism of wrinkle formation can be well understood based on the continuous elastic medium theory (Föppl−von Kármán plate equations).[2,3] The in-plane wrinkle period (or wavelength) is dependent on the film thickness and the film−substrate modulus ratio under small strain conditions. The out-of-plane amplitude is directly proportional to the wavelength and the square root of strain. The wrinkle orientation and ordering can be controlled by tuning the local stress field and loading history.[4−6] The controllable wrinkle patterns have been widely applied in various engineering fields such as stretchable electronics, tunable optics, surface wetting, friction and adhesion, smart materials, energy devices, information storage, biomedicines, microfluid handling systems, and so on.[7−10]

The wrinkle wavelength and amplitude are uniform for a homogeneous film−substrate system (with the same film thickness and material parameters). The strain energy is evenly distributed on the homogeneously wrinkled surface. As the compressive strain increases greatly, however, the wrinkle mode becomes unstable and it may evolve into advanced instability modes such as crease,[11] fold,[12] period-double,[13] and ridge,[14] depending on the film−substrate modulus ratio.[15,16] The advanced instability modes are always accompanied by the redistribution and localization of the strain energy at very small film regions.[11−14] Among these advanced instability modes, the ridge pattern usually occurs in the cases of large film−substrate modulus ratio and large substrate prestretch.[17−21] The theoretical analysis and numerical simulation predict that the ridge pattern usually exhibits separated protrusions evolving from wrinkle crests.[17−20] However, distinct surface structures in the form of alternating packets of large and small undulations can also be observed in some experiments.[14,22,23] Furthermore, both experimental and theoretical studies show that the critical strain for the formation of ridge pattern is only slightly larger than the critical wrinkling strain in some cases,[18,19] indicating that the wrinkles and ridges may be coexisting and coevolutionary in a real film−substrate system.

Received: September 7, 2023
Revised: November 7, 2023
Accepted: December 4, 2023
Published: December 28, 2023

ACS Publications © 2023 American Chemical Society

https://doi.org/10.1021/acs.langmuir.3c02655
Langmuir 2024, 40, 403−412

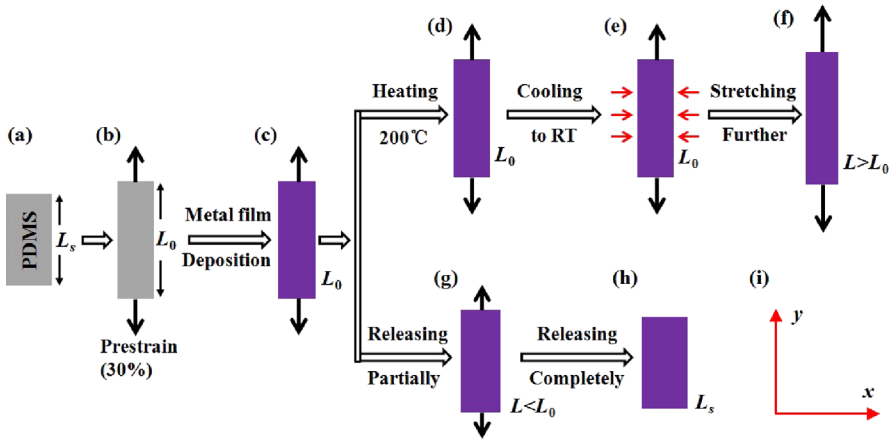

Figure 1. Schematic drawing of film preparation and strain loading. (a) Pristine PDMS sheet. (b) PDMS sheet was stretched to a strain of 30%. (c) Silver film was deposited on the prestretched PDMS. (d) Sample was annealed at 200 °C for 20 min. (e) Sample was naturally cooled down to room temperature. The red arrows denote the uniaxial compression. (f) PDMS was further stretched to a random length after cooling. (g) The unannealed sample was directly compressed by partially releasing the prestrain. (h) Prestrain was released completely. (i) Definition of the x and y axes.

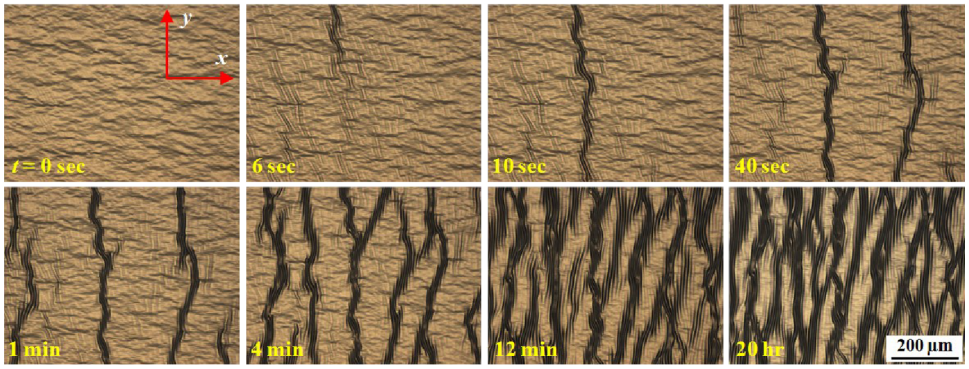

Figure 2. In situ morphological evolution of the sample with h = 90 nm during the cooling process. The data appearing in the bottom-left corners represent the cooling time t. All images have the same size of 695 × 521 μm^2.

Although the structure and mechanics of the ridge pattern (especially the wrinkle-to-ridge transition) have been extensively investigated in the past decade,[14,17−21] the details about the coexistence, coevolution, and interaction of wrinkles and ridges are still unclear up to now. Here, we report on the formation and evolution of coexisting wrinkle and ridge patterns in metal films deposited on PDMS substrates by uniaxial compression. It is found that the strain energy is not evenly distributed in the film surface at small strain conditions, resulting in the spontaneous formation of coexisting wrinkle and ridge patterns in the form of alternating packets of large and small undulations. Such patterns are different from the theoretical predications[17−20] but are analogous to some experimental observations.[14,22,23] As the strain increases, they evolve into a sinusoidal-like mode with a high aspect ratio gradually via nonuniform growth of the undulation amplitudes. This process can be attributed to the redistribution and real-time evolution of the strain energy across the film surface, which has not been reported previously.

EXPERIMENTAL SECTION

We deposited metal films on soft PDMS substrates to construct a film−substrate bilayer system. The PDMS was prepared by curing a 10:1 mass ratio of prepolymer and curing agent at 80 °C overnight. The PDMS sheet with ∼30 × 15 mm^2 in-plane size and ∼1.2 mm thickness was mounted on a custom-designed stretching device and was stretched to a prestrain of 30% (prestretch 1.3), as shown in Figure 1a,b. Then, metal (silver in the main text) films were deposited on the prestretched PDMS substrates by a direct current magnetron sputtering technique at room temperature, as shown in Figure 1c. The film thickness was controlled by the deposition rate (here it was fixed at 0.5 nm/s) and the deposition time.

After deposition, we adopted two methods to generate uniaxial compressive stress and induce surface instability of the film: (1) the sample was annealed at 200 °C for 20 min at the prestrain state, as shown in Figure 1d. During this process, the silver film underwent a plastic deformation or viscous flow at the interface and kept conformal to the PDMS without cracking.[23,24] Subsequently, natural cooling generated uniaxial compressive stress in the x direction and induced surface instability, as shown in Figure 1e. The thermal stress could be conveniently controlled by changing the annealed temperature.[23] To avoid obvious mechanical damage to PDMS under high temperatures, the annealed temperature was fixed at 200 °C in this study. After cooling, the PDMS can be further stretched to increase the uniaxial compressive stress in the x direction, as shown in Figure 1f. (2) The prestrain of PDMS was released gradually to generate uniaxial compressive stress in the y direction, as shown in Figure 1g,h. Note that these two methods lead to similar experimental results. They had their respective advantages and disadvantages. The annealing-induced stress was continuously changed and the *in situ* morphological evolution can be conveniently detected. However, the thermal stress was limited by the annealing temperature. On the contrary, the mechanical loading had a larger strain range, and the entire process of morphological evolution could be achieved.

https://doi.org/10.1021/acs.langmuir.3c02655
Langmuir 2024, 40, 403−412

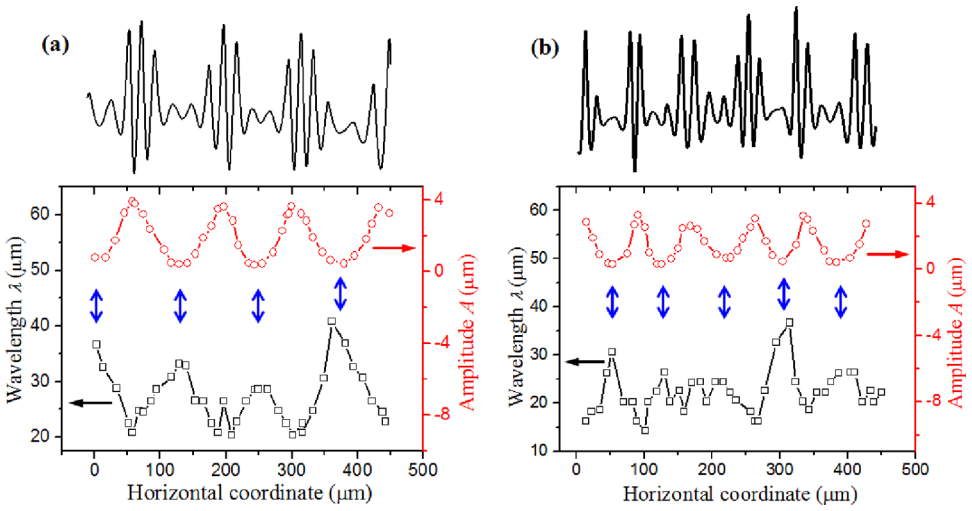

Figure 3. Spatial distributions of the wavelength λ and amplitude A of coexisting wrinkle and ridge patterns for the two samples. The top images show the corresponding sectional profiles: (a) h = 150 nm; (b) h = 120 nm.

The film morphologies were detected by an optical microscope (Olympus BX41) and an atomic force microscope operated in tapping mode (AFM, JPKSPM). The cross-sectional profiles were detected by a stylus profiler (DektakXT, Bruker).

RESULTS AND DISCUSSION

Heating/Cooling Cycle. After annealing at 200 °C for 20 min, the sample was placed under an optical microscope for morphological detection. The in situ morphological evolution of the sample during natural cooling is shown in Figure 2 (for details, see Movie S1). We find that the film surface forms tiny wrinkles along the x direction at t = 0. They originate from the slight compressive stress during heating. In our experiment, the substrate length is constrained by two clamps and thus the film strain in the y direction is almost unchanged during temperature variation. In the x direction, however, the expansion of PDMS is unrestricted due to the free boundary condition (see Figure 1). As elapsed time increases, the sample gradually cools from 200 °C to room temperature. Because the thermal expansion coefficient of PDMS is much larger than that of silver, the PDMS thermally contracts and places the film under uniaxial compressive stress in the x direction. The compressive stress increases with the elapsed time, leading to the formation of striped patterns along the y direction.

The thermal strain of a bilayer system ε_{th} is easily estimated based on the formula $\varepsilon_{th} = (\alpha_s - \alpha_f)\Delta T$, where ΔT is the temperature variation, α_f and α_s are the thermal expansion coefficients of the film and substrate, respectively.[1] In this experiment, $\alpha_f = 2.0 \times 10^{-5}$ K^{-1} (Ag), $\alpha_s = 3.2 \times 10^{-4}$ K^{-1} (PDMS) and ΔT = 180 K. Thus, the thermal strain is estimated to be about 5.4%. As the compressive strain is beyond a critical value, wrinkles first form on the film surface. The continuous elastic medium theory predicts that the critical wrinkling strain is expressed as[1,2]

$$\varepsilon_w^c = \frac{1}{4}\left[\frac{3E_s(1-\nu_f^2)}{E_f(1-\nu_s^2)}\right]^{2/3} \quad (1)$$

where E_f, E_s, ν_f, and ν_s are the elastic moduli and Poisson's ratios of the film and substrate, respectively. The critical wrinkling strain for the Ag/PDMS system is much smaller (~0.05%) because of the large modulus mismatch (E_f = 70 GPa and E_s = 2 MPa). Therefore, wrinkles are easily induced by thermal treatment or mechanical loading in metal film−PDMS systems.

It can be seen from Figure 2 that the striped patterns are not uniform but localized remarkably. At t = 6 s, some tiny wrinkles along the y direction can be observed and they evolve into a localized pattern quickly. This localized pattern behaves like a snapping process and has a larger amplitude compared with the neighboring waves (for details see below), indicative of the ridge mode.[17−21] The quick transition from wrinkling to ridging indicates that the critical strain for the formation of a ridge pattern is only slightly larger than the critical wrinkling strain in our experiment.[18,19] From t = 6−10 s, an isolated ridge pattern propagates from top to bottom. At t = 40 and 60 s, the second and third localized ridges appear in the image in sequence. As the time further increases, more ridge patterns form, leading to a progressive decrease in the average spacing of localized ridges (see Figure S1). Our experiment shows that when the cooled sample is heated to 200 °C again, the ridge patterns disappear completely. But they are recovered during subsequent cooling (see Figure S2). This test indicates that such a pattern is reversible by the heating/cooling cycle.

Morphological Features. To discover the morphological features of the localized ridges, cross-sectional profiles are detected by the stylus profiler after cooling, as shown in Figure 3. It is clear that the surface patterns exhibit the form of alternating packets of large and small undulations.[14,22,23] A single packet usually contains 3−5 wave periods initially. The largest amplitude corresponds to the ridge center, while the smaller undulations between the neighboring ridges are still in wrinkle mode. Therefore, the heterogeneous surface can be viewed as a mixture of localized ridges and coexisting wrinkles. Figure 3 also shows the spatial distributions of wrinkle or ridge amplitudes and wavelengths for two samples with film thicknesses of h = 150 and 120 nm. It is clear that the amplitudes are quasi-periodically oscillatory. They successively change from near zero to ~4 μm (for h = 150 nm) or ~3 μm (for h = 120 nm). Unlike the homogeneous wrinkles, whose wavelengths are uniformly distributed, the wavelengths of such patterns are also obviously oscillatory. The peaks of wavelengths are always consistent with the troughs of amplitudes, as denoted by the bidirectional arrows in Figure 3.

https://doi.org/10.1021/acs.langmuir.3c02655
Langmuir 2024, 40, 403−412

We suggest that this phenomenon results from the following two reasons. First, the continuous elastic medium theory predicts that the wrinkle wavelength at critical strain can be expressed as[1−3]

$$\lambda_w^c = 2\pi h\left[\frac{E_f(1-\nu_s^2)}{3E_s(1-\nu_f^2)}\right]^{1/3} \quad (2)$$

For large strain condition, the wrinkle wavelength needs to be corrected as[16,25]

$$\lambda_w = \lambda_w^c\frac{1-\varepsilon}{1-\varepsilon_w^c} \quad (3)$$

where ε is the compressive strain. The wrinkle amplitude can be expressed as[1−3]

$$A_w = h\left(\frac{\varepsilon}{\varepsilon_w^c}\right)^{1/2} \propto \lambda_w^c\sqrt{\varepsilon} \quad (4)$$

The ridge pattern originates from the quick growth of a wrinkle crest. The ridge width (or wavelength) is equal to the wrinkle wavelength initially, but it needs to consider the strain effect. The ridge wavelength and amplitude are expressed as[15,16]

$$\lambda_r = \lambda_w^c\frac{1-\varepsilon}{1-\varepsilon_w^c} \quad (5)$$

$$A_r = \lambda_w^c[0.24(\varepsilon-\varepsilon_w^c)+0.075] \quad (6)$$

Note that the wrinkle wavelength and ridge wavelength have the same expression but the compressive strains (ε) are different. Eq 4 gives $\varepsilon \propto A_w^2$, indicating that the compressive strain is not evenly distributed in the heterogeneous film surface. The strain is highly concentrated at the localized ridges due to the large amplitudes. According to eqs 3 and 5, the wrinkle or ridge wavelength may decrease steadily with increasing compressive strain. Therefore, the locations of the minimum amplitudes (i.e., minimum strains) are always consistent with the locations of the maximum wavelengths and vice versa. Second, the ridge patterns first form and remain stable at the localized positions, and then wrinkles appear in small strain regions between the neighboring ridges. Due to the staggered manner of the localized ridges,[22] more wrinkle impurities such as bifurcations and terminations[26,27] can exist in the small strain regions, leading to the increase of wrinkle wavelength.

Figure 4 shows the evolution of coexisting wrinkle and ridge patterns with increasing film thickness taken by AFM. It is clear that the surface morphologies for different film thicknesses are self-similar. However, the wrinkle or ridge dimensions increase obviously with the film thickness. In our experiment, the material parameters of the film and substrate, the thermal strain, and the critical wrinkling strain are all constant. Therefore, the wrinkle or ridge dimensions (wavelength and amplitude) are all directly proportional to the film thickness based on eqs 2−6, which is consistent with the previous studies.[18,23,24]

Evolution by Further Stretching. After heat treatment, we detected the evolution of the coexisting wrinkle and ridge patterns via further uniaxial stretching along the y direction. The in situ evolution of the film morphologies under mechanical stretching is shown in Figure 5a. It is clear that

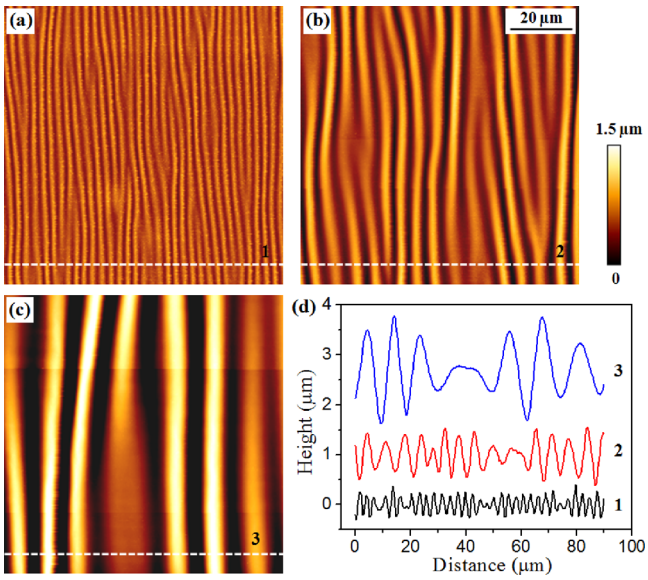

Figure 4. AFM images (a−c) and corresponding profile lines (d) of the coexisting ridge and wrinkle patterns with different film thicknesses after cooling. (a) h = 15 nm; (b) h = 30 nm; (c) h = 60 nm. All images have the same size of 90 × 90 μm^2.

the tensile strain leads to the formation of parallel cracks along the x direction.[28,29] The critical tensile strain for crack formation is $\varepsilon_{ten} = \varepsilon_{app}$ = 2.8%, where ε_{app} is the applied mechanical strain. Then, the number density and width of the cracks increase gradually to accommodate more tensile strain energy. On the other hand, a compressive strain will be generated in the x direction due to the Poisson's effect of PDMS (ν_{PDMS} = 0.5). As the compressive stress increases, the localization phenomenon becomes obscure gradually.

Figure 5b shows the cross-sectional profiles of the surface morphologies under different compressive strains. Here, the total compressive strain is expressed as $\varepsilon_{com} = \varepsilon_{th} + \nu_{PDMS}\cdot\varepsilon_{app}$. We find that the film surface is obviously heterogeneous or localized just after cooling ($\varepsilon_{com} = \varepsilon_{th}$ = 5.4%). As the compressive strain increases, the amplitude inhomogeneity decays gradually, and finally a sinusoidal-like mode is formed. To further understand the evolution behaviors of coexisting wrinkle and ridge patterns, we measured the dependence of the wrinkle and ridge amplitudes on the total compressive strain, as shown in Figure 5c. Here, the maximum and minimum amplitudes are viewed as ridge amplitude A_r and wrinkle amplitude A_w, respectively. We find that when ε_{com} < 15% (stage II), the ridge amplitude A_r is almost unchanged while the wrinkle amplitude A_w increases successively with increasing ε_{com}. At ε_{com} ∼ 15%, the ridge amplitude and wrinkle amplitude become indistinguishable in the experiment due to the formation of a sinusoidal-like pattern. As ε_{com} further increases (stage III), the amplitude of the sinusoidal-like pattern A_s increases steadily.

Uniaxial Mechanical Compression. It raises the question of whether heat treatment is necessary for the formation of the coexisting wrinkle and ridge patterns. To answer this question, we performed an alternative test in which direct compression was applied (no heat treatment). The in situ morphological evolution of the film under direct compression is shown in Figure 6. We find that the as-prepared sample is free of wrinkles. Upon application of a very small mechanical compression, localized ridge patterns appear in the film,

https://doi.org/10.1021/acs.langmuir.3c02655
Langmuir 2024, 40, 403−412

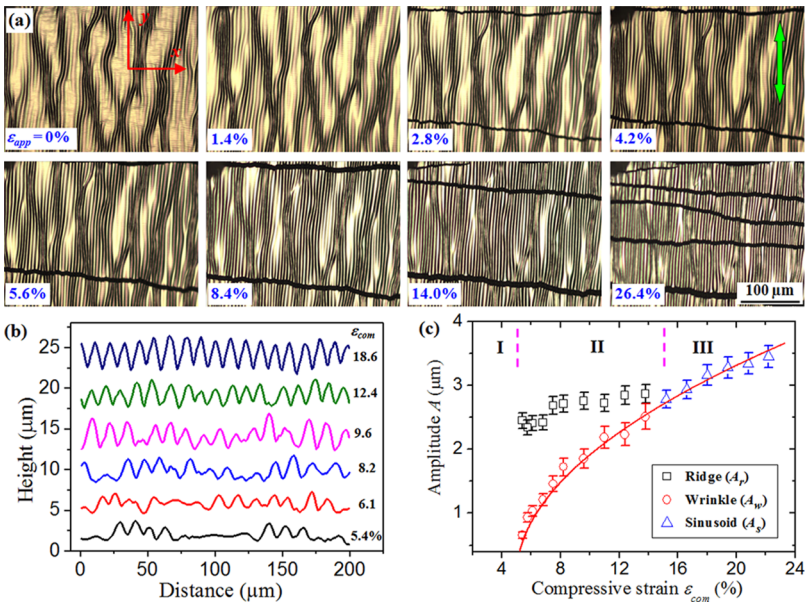

Figure 5. (a) In situ morphological evolution of the annealed sample with h = 90 nm by further uniaxial stretching after cooling. The data appearing in the bottom-left corners represent the applied mechanical strain along the y direction. All images have the same size of 348 × 261 μm^2. (b) Evolution of the cross-sectional profile with increasing total compressive strain expressed as $\varepsilon_{com} = \varepsilon_{th} + \nu_{PDMS}\cdot\varepsilon_{app}$. (c) Evolution of the amplitudes A_r, A_w, and A_s with the compressive strain ε_{com}. The solid line is a fit to the experimental data of A_w and A_s by $A \propto \sqrt{\varepsilon - \varepsilon_c'}$ with a constant ε_c' = 5%.

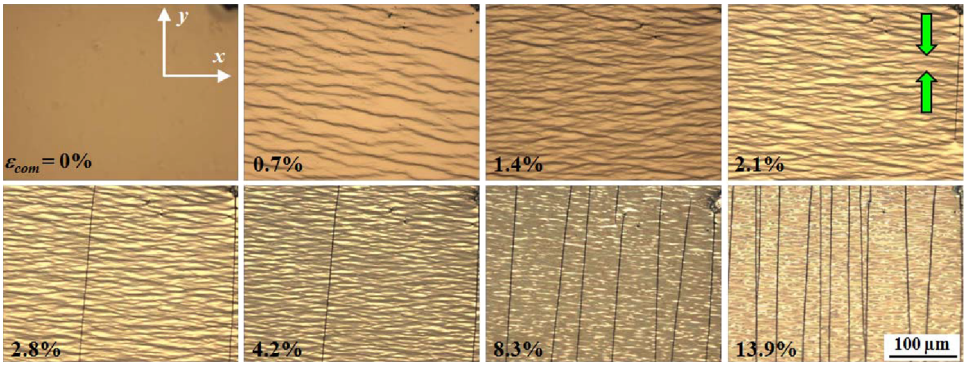

Figure 6. In situ morphological evolution of the sample with h = 30 nm via direct uniaxial compression (no annealing treatment). The data appearing in the bottom-left corners represent the compressive strain, which is equal to the applied mechanical strain along the y direction. All images have the same size of 348 × 261 μm^2.

similar to those induced by heat treatment, as shown in Figures 2 and 5. Our experiment shows that other metal films sputter-deposited on PDMS substrates also lead to a similar phenomenon (see Figure S3), indicating that the localized ridge patterns are universal for metal film−polymer substrate systems. As the compression increases, the number density of localized ridges increases. At $\varepsilon_{app} \sim 2.1\%$, cracks along the y direction form due to the tensile strain in the x direction induced by Poisson's effect.[28,29] Note that the critical tensile strain for crack formation, in this case, is about $\varepsilon_{ten} = \nu_{PDMS}\cdot\varepsilon_{app} = 1.1\%$, which is smaller than that shown in Figure 5 due to the smaller film thickness in Figure 6.

Figure 7a shows the cross-sectional profiles of the film surface under different compressive strains by mechanical loading. We find that the sectional profile at $\varepsilon_{com} = 0$ is flat and wrinkle-free. Then localized ridges start to form in some regions, while the film surface between neighboring ridges remains flat. As the compressive strain increases, the number density of localized ridges increases gradually and the average spacing decreases successively, as shown in Figure 7b. Finally, the amplitude inhomogeneity disappears, and a sinusoidal-like pattern is formed. Figure 7c shows the dependence of the wrinkle and ridge amplitudes on the compressive strain. It is clear that the total region can be divided into three stages.

In stage I ($\varepsilon_{com} < 5\%$), A_w approaches zero while A_r increases approximately linearly with strain. It can be seen from Figure 7b that the average spacing of localized ridges decreases obviously in stage I. That is, the localized ridges are not saturated in this stage. The compressive strain is released by increasing the number density and amplitude of the ridge patterns simultaneously. In stage II ($5\% < \varepsilon_{com} < 15\%$), A_r is almost unchanged while A_w increases successively with strain. In this stage, the localized ridges have been saturated, and the average spacing is almost unchanged (see Figure 7b). The compressive strain is released by increasing wrinkle amplitude solely. As a result, a sinusoidal-like pattern appears at $\varepsilon_{com} \sim 15\%$. In stage III ($\varepsilon_{com} > 15\%$), the amplitude of the sinusoidal-like pattern increases steadily with strain. By comparison of the

https://doi.org/10.1021/acs.langmuir.3c02655
Langmuir 2024, 40, 403−412

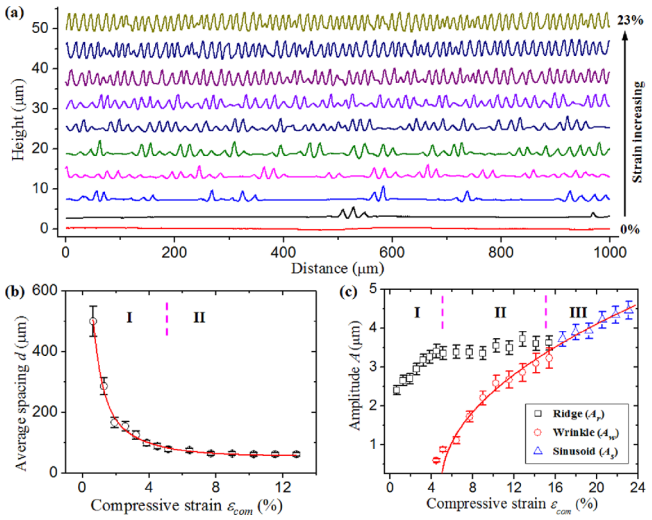

Figure 7. (a) Evolution of the cross-sectional profile with increasing compressive strain by uniaxial mechanical loading in the sample with h = 90 nm. (b) Evolution of the average spacing of localized ridges d with ε_{com}. The solid line is a guide to the eye. (c) Evolution of the amplitudes A_r, A_w, and A_s with ε_{com}. The solid line is a fit to the experimental data of A_w and A_s by $A \propto \sqrt{\varepsilon - \varepsilon_c'}$ with ε_c' = 5%.

results shown in Figures 5c and 7c, it can be concluded that the evolution behaviors via cooling plus stretching (method 1) and direct compression (method 2) are similar. In method 1, stage I occurs in the cooling process and is induced by the thermal strain. It is missing in Figure 5c because the evolution of the sectional profile during cooling is hard to measure in the experiment.

Evolution Mechanism. Localized patterns can be widely observed in natural and artificial systems. For example, the tensile strain leads to the formation of localized cracks in brittle materials such as drying mud, coatings, and films.[30,31] The compressive strain leads to the formation of localized buckle-delaminations in elastic films on rigid substrates.[32,33] For soft elastic substrates, the coexistence of sinusoidal wrinkles and localized buckle-delaminations can be observed if the interfacial adhesion is comparatively weak.[34−36] For liquid or very soft substrates, the elastic films tend to form sinusoidal wrinkles under modest compression and localized folds,[37] ridges,[21] or period-doubles[13] at large strain. For pure soft materials such as gels, hydrogels, and biological tissues, localized creases are observed under large compression.[11]

It is now well-known that the localized patterns originate from strain localization. The coexisting wrinkle and ridge patterns presented in this work are also induced by strain localization. In stage I, the applied compressive strain is first localized at some positions mainly due to the film imperfections, leading to a quick increase of local amplitudes. The increase in amplitude further enhances the structural inhomogeneity and localizes the strain energy. Therefore, once the localized ridge initiates at a certain position, it can spontaneously propagate to form a stable structure with large amplitude, as shown in Figure 2. This situation is similar to other localized patterns such as cracks, buckle-delaminations, and creases.[11,30−36] Note that the ridge formation can be viewed as a snapping process, as shown in Figures 2 and 6. The wrinkled or even flat film surface can abruptly bump up to a certain height.[19] Therefore, the ridge amplitude has a larger value at a very small strain, as shown in Figure 7c. Furthermore, eq 6 shows that the ridge amplitude increases linearly with compressive strain, consistent with the experimental result as shown in Figure 7c.

After the localized ridges form, the residual strain is not evenly distributed on the film surface. The strain in the region between two neighboring localized ridges is largest because the ridge patterns can relax local strain effectively.[14,17−21] Therefore, new localized ridges tend to initiate in the middle regions, and their spacing is almost uniform. When the spacing of localized ridges decreases to a certain value, the localizing is saturated, and no new ridge pattern forms thereafter. At this point, the ridge amplitude has increased greatly while the wrinkle amplitude in the middle regions is still close to zero, indicating that the strain localization reaches its peak.

Then, in stage II, the ridge amplitude remains unchanged while the wrinkle amplitude increases successively, leading to the gradual decay of the strain localization. Note that the wrinkle amplitude increases from zero and no snapping phenomenon is observed (see Figure 7c), which is completely different from the localized ridge. Figure 7c also shows that the wrinkle amplitude is directly proportional to the square root of strain, consistent with the well-known amplitude−strain relation as shown in eq 4. Recently, Chen and Crosby[38] investigated the amplitude growth of a periodically wrinkled film surface comprising flat and uniformly wrinkled regions. They found that the wrinkle amplitude of the flat region increases quickly while that of the wrinkled region increases slowly with increasing applied strain, leading to the formation of uniform amplitudes finally, which is quite similar to our experimental results in stage II. However, the initial heterogeneous surface patterns are artificial in the previous work[38] while they are spontaneous in our experiment.

In stage III, the strain localization disappears completely, and a sinusoidal-like pattern is formed. The amplitude of the sinusoidal-like pattern increases continuously with increasing strain. Furthermore, the experimental data of A_s are also fitted by the well-known amplitude-strain relation, as shown in Figures 5c and 7c. The precise amplitude−strain relation in this work should be corrected as $A \propto \sqrt{\varepsilon - \varepsilon_c'}$, where ε_c' is the critical strain for initiation of minimum wrinkle amplitudes, i.e., the transition point from stage I to stage II (here $\varepsilon_c' \approx 5\%$). For the sample shown in Figure 7, the amplitude and wavelength of the sinusoidal-like pattern at ε_{com} = 23% are about 4.5 and 14 μm, respectively. Thus, the aspect ratio of such a pattern is about 0.32, which is much larger than that of common wrinkles (typically ∼0.1). The previous studies showed that the aspect ratio can be beyond 0.5 when the prestrain increases.[17,20,39] It is well-known that the ridge mode can delay or suppress the formation of other localized patterns such as period-double and fold and thus can increase the aspect ratio greatly.

Finally, it should be noted that the profiles of traditional ridges and our experimental observations have some discrepancies. The traditional ridge mode usually has a single protrusion evolving from a wrinkle crest, while our experiment exhibits a distinctly heterogeneous pattern with oscillatory amplitude and wavelength. Although the structure of alternating packets of large and small undulations has been observed in some experiments,[14,22,23] the mechanisms of formation and evolution of such pattern are still unknown. Recently, Xu's group theoretically obtained similar alternating packet structures in the cases of large prestretch (∼1.8) and small film−substrate modulus ratio (45−200).[40,41] But these

https://doi.org/10.1021/acs.langmuir.3c02655
Langmuir 2024, 40, 403−412

formation conditions are different from our experiment with comparatively small prestretch (1.3) and extremely large modulus ratio (above 10^4). Further theoretical and simulation research is needed to illuminate the mechanisms of spontaneous strain localization and heterogeneous patterns with oscillatory amplitude and wavelength in a real film−substrate system.

Finite Element Simulations. To further understand the formation and evolution of ridges (stage I) and secondary wrinkles (stage II), nonlinear finite element simulations (FEM) are employed. Previous studies elucidated that the formation of ridge is strongly influenced by prestretching[19,42] and modulus ratio between film and substrate.[40] For a film−substrate system with a large modulus ratio μ_f/μ_s, localized ridges prevail when a sufficiently large prestretch ε_{pre} is adopted.

The commercial software Abaqus is adopted to perform nonlinear FEMs under plane strain conditions. A prestretched film−substrate system is employed to investigate the formation of localized ridges under overall compressive strain (stage I), as shown in Figure 8a. Since the evolution of coexisting wrinkle and ridge patterns (stage II) requires large compressive strains, in order to ensure convergence in the postbuckling analysis, a film−substrate system with preset initial localized ridges is built to simulate the formation and evolution of the secondary wrinkles in ridged system, as shown in Figure 8b. The detailed parameters of the finite element models are described below: the thickness of the film is h = 90 nm, and the thickness of the substrate is set as $H = 200\,h$. Since H is much larger than h, the substrate can be considered as semi-infinite, and the buckling behaviors are not affected by the bottom of the substrate. The lengths of the prestretched system and preset ridged system are L_1/h = 675 and L_2/h = 919, respectively. The length is set to ensure that $L \geq 5\lambda$, where λ is the theoretical wrinkle wavelength. The prestretch strain is ε_{pre} = 60% to ensure that the localized ridges occur when compressive strain ε exceeds a critical value. The geometric parameters of preset ridges are a/h = 32 and b/h = 34, according to the simulated results of stage I. The bottom of the substrate has zero vertical displacement and no shear traction. Symmetry boundary condition is set about the plane x = 0 and on the right edge $x = L_1, L_2$. A prescribed uniform horizontal displacement is imposed to create compressive strain ε.

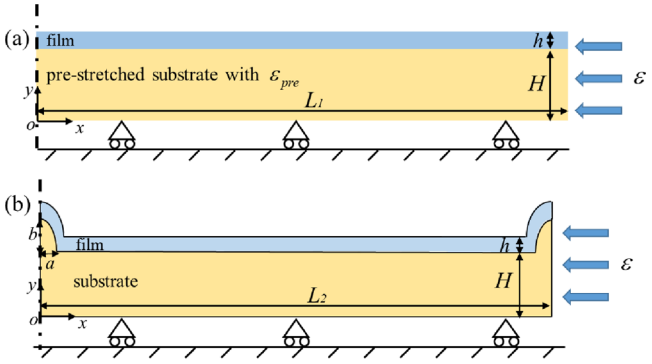

Figure 8. Schematic diagram of the film−substrate system under plane strain conditions. (a) Model to simulate the formation of localized ridges (stage I). A stiff film is bonded to a relatively compliant prestretched substrate with ε_{pre}. (b) Model to simulate the formation and evolution of wrinkles on a ridged film−substrate system (stage II). Two initial localized ridges are preset in the system.

Both the film and substrate are incompressible neo-Hookean materials, and the ground shear moduli are μ_f and μ_s, respectively. The modulus ratio between the film and substrate is set as μ_f/μ_s = 35,000, according to the materials used in experiments. The 4-node bilinear hybrid plane strain elements with reduced integration (CPE4RH) are employed for both the film and substrate to explore the buckling behaviors of the film−substrate system under plane strain conditions. More than 10 girds are adopted within one wavelength along the x direction. Along the thickness direction, the film and substrate are meshed with 4 grids and 30 grids, respectively. In simulations, a linear perturbation procedure is accomplished first to obtain the buckle modes of the system. The first-order critical eigenmode scaled by a very small factor of $\delta = 0.01h$ is introduced into the system as a geometric imperfection to trigger both wrinkles and localized ridges. The pseudo-dynamic method is adopted to obtain the postbuckling behaviors of the system. The damping factor is set as 0.0002 in the simulations to ensure convergence.

The process of localized ridge formation is shown in Figure 9. When an increasing compressive strain is applied to a prestretched film−substrate system, both the film and substrate will undergo out-of-plane displacements to release the strain. When ε proceeds through the critical strain of wrinkling ε_w^c, the uniform striped wrinkles occur, and each wrinkle has the same wavelength and amplitude. At ε = 5%, we can see a ridge starts to form at the right end, and the amplitudes of the wrinkles near the ridge are reduced. At ε = 12%, a second ridge forms, and the wrinkles almost disappear. The evolution of the cross-

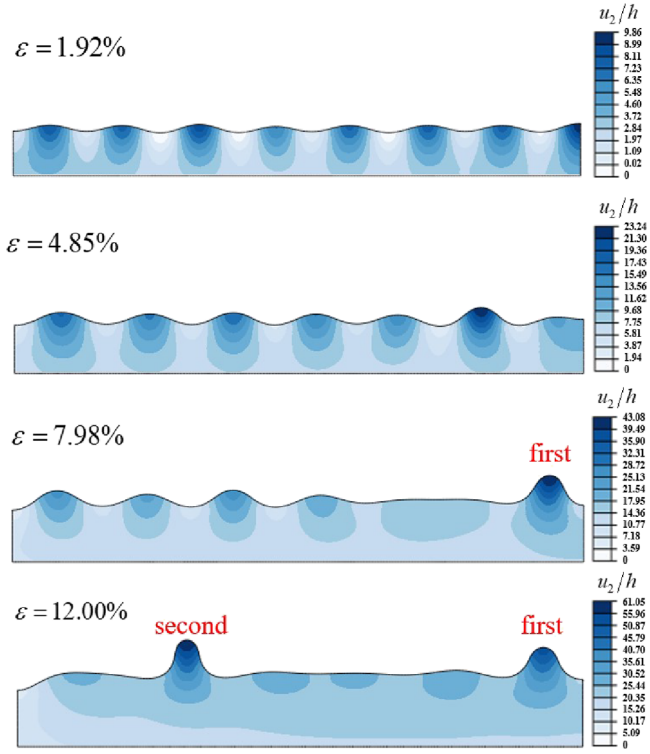

Figure 9. Evolution of wrinkling and formation of localized ridges under plane compressive strain ε, where the prestretch ε_{pre} = 60%. The color bar represents the dimensionless out-of-plane displacement u_2/h. Only the upper part of the substrate is shown.

https://doi.org/10.1021/acs.langmuir.3c02655
Langmuir 2024, 40, 403−412

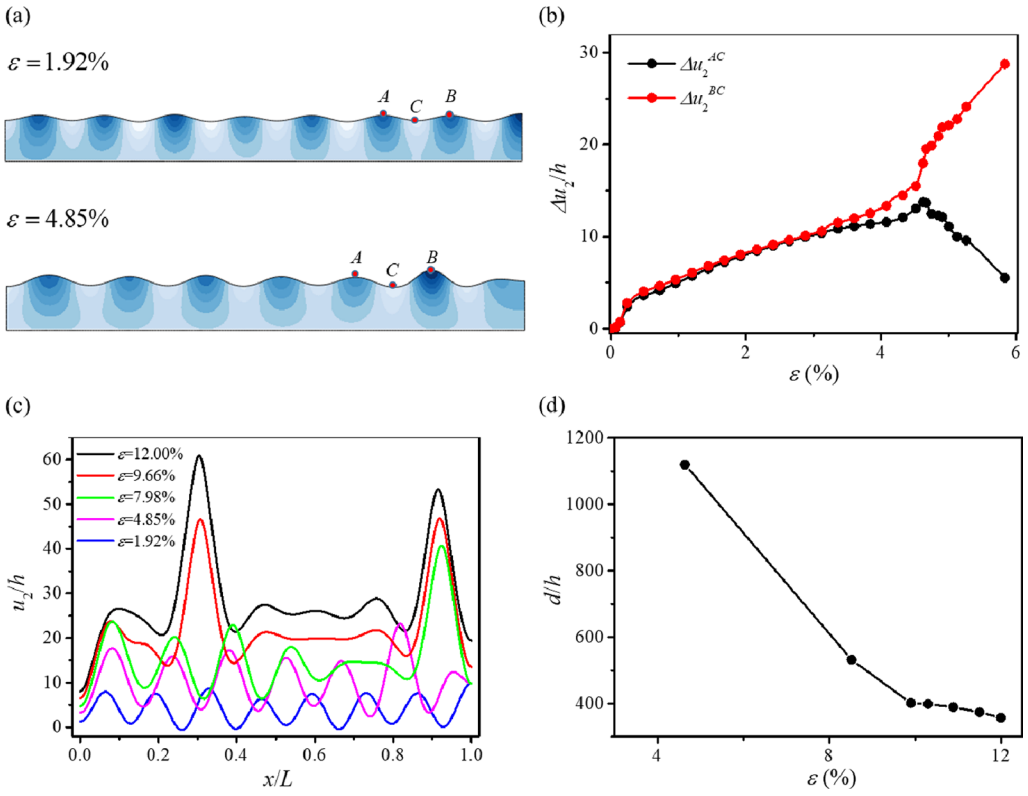

Figure 10. (a) Wrinkle patterns of the film−substrate system at ε = 1.92 and ε = 4.85%. Points A and B are the positions of two adjacent wrinkle peaks, and point C is the position of the valley between them. Only the upper part of the substrate is shown. (b) Evolution of dimensionless relative out-of-plane displacement $\Delta u_2/h$ with ε. (c) Evolution of the cross-sectional profile with increasing compressive strain. (d) Evolution of the dimensionless average spacing of localized ridges d/h with ε.

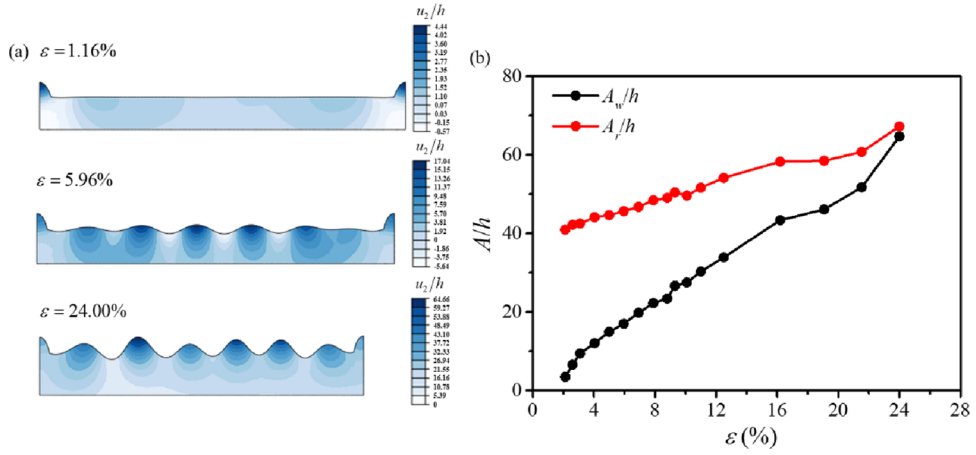

Figure 11. (a) Evolution of wrinkle patterns of the film−substrate system with preset initial localized ridges with ε. The color bar represents the dimensionless out-of-plane displacement u_2/h. Only the upper part of the substrate is shown. (b) Evolution of dimensionless amplitudes A_r/h and A_w/h with ε in stage II.

sectional profile in Figure 10c demonstrates this process clearly.

To further understand the evolution from wrinkles to localized ridges, we select two adjacent wrinkles and define the dimensionless relative out-of-plane displacement as $\Delta u_2^{AC}/h = (\Delta u_2^A - u_2^C)/h$ and $\Delta u_2^{BC}/h = (\Delta u_2^B - u_2^C)/h$, as shown in Figure 10a. When ε < 3%, it is clear that the relative displacements of positions A and B are nearly equal and increase gradually. In this case, the striped wrinkles remain uniform. However, when ε > 3%, the two curves begin to diverge, as shown in Figure 10b. It is found that the relative displacement of position B is further increased, while the displacement of position A begins to decay after an increase to an extreme value. As the compressive strain ε increases, wrinkle B evolves into a ridge, while wrinkle A gradually disappears. We can speculate that the critical strain from wrinkle to ridge is about 3% in this case. We can see in Figure 10d that since the ridges are formed one after another, the average spacing of the ridges will first drop sharply and then decrease slowly as the strain increases, which is in good agreement with the experimentally observed result as shown in Figure 7b.

https://doi.org/10.1021/acs.langmuir.3c02655
Langmuir 2024, 40, 403−412

The evolution of wrinkles on the film−substrate system with preset ridges is shown in Figure 11a. As the compressive strain increases, the wrinkles are first formed far away from the ridges and gradually spread around the ridges. Due to the finite deformation effect,[16,25,43] the wavelength of the wrinkles decreases while the amplitude increases as the strain increases. We can see in Figure 11b that the wrinkle amplitude A_w/h increases sharply with the increase of strain, while the amplitude of the ridge A_r/h increases slowly, and the wrinkle amplitude increasingly approaches the amplitude of the ridge, which is in good agreement with the experimental observations, as shown in Figure 7c. Finally, it should be emphasized that although the FEM simulations have captured the primary results observed in experiments, some discrepancies between theory and experiment still existed. First, the prestrain for the formation of ridges in simulations (60%) is larger than that in experiments (30%). Smaller prestrain usually leads to the formation of other instability modes (e.g., period doubling[13,15]) in theory. Second, the distinct form of alternating packets of large and small undulations observed in experiments is not obtained by FEM simulations. Third, the three-stage evolution process presented in this study cannot be achieved directly by FEM simulations. We believe that these discrepancies originates from the difference between the ideal system and the real film system.

CONCLUSIONS

In summary, a distinct surface instability mode composed of alternating packets of large and small undulations can be observed in metal films deposited on PDMS substrates. The dynamic evolutions of such coexisting wrinkle and ridge patterns are described in detail. The strains are modulated by two techniques: thermal treatment under a prestrain state followed by further mechanical stretching (method 1) and direct mechanical compression (method 2), both leading to similar experimental results. The entire evolution process can be divided into three stages. In the first stage (below 5% strain), the number density and amplitude of localized ridges increase simultaneously, while the minimum wrinkle amplitude between neighboring ridges is still close to zero. In the second stage (from 5 to 15% strain), the ridge amplitude remains unchanged while the wrinkle amplitude increases successively in compliance with the classical amplitude−strain formula. In the third stage (above 15% strain), a sinusoidal-like mode forms, and its amplitude increases steadily with increasing strain further. The formation and evolution of coexisting wrinkle and ridge patterns can be attributed to the redistribution and real-time evolution of the strain energy across the film surface under mechanical loading. This work can provide a deep insight into the morphological feature and mechanical mechanism of such unique instability mode driven by strain localization (initially) and homogenization (last) in a hard film−soft substrate system. The facile experimental technique can be adopted to fabricate various heterogeneous patterns with different profiles, which are beneficial for engineering applications.

ASSOCIATED CONTENT

Supporting Information

The Supporting Information is available free of charge at https://pubs.acs.org/doi/10.1021/acs.langmuir.3c02655.

Evolutions of the number and average spacing of localized ridges during the cooling process; in situ morphological evolution of the sample during the second cooling process; localized ridge patterns in other metal films (including Cu, Mo, Zn, and Fe) on PDMS substrates; detailed evolution of the cross-sectional profile by uniaxial mechanical loading (PDF)

Dynamical evolution of the sample during the cooling process (MP4)

AUTHOR INFORMATION

Corresponding Authors

Senjiang Yu − *Key Laboratory of Novel Materials for Sensor of Zhejiang Province, College of Materials and Environmental Engineering, Hangzhou Dianzi University, Hangzhou 310018, P.R. China;* orcid.org/0000-0001-9411-6458; Email: sjyu@hdu.edu.cn

Yong Ni − *CAS Key Laboratory of Mechanical Behavior and Design of Materials, Department of Modern Mechanics, University of Science and Technology of China, Hefei 230026, P.R. China; State Key Laboratory of Nonlinear Mechanics, Institute of Mechanics, Chinese Academy of Science, Beijing 100190, P.R. China;* orcid.org/0000-0002-8944-5764; Email: yni@ustc.edu.cn

Authors

Jiahui Zhang − *CAS Key Laboratory of Mechanical Behavior and Design of Materials, Department of Modern Mechanics, University of Science and Technology of China, Hefei 230026, P.R. China*

Hong Zhou − *Department of Physics, China Jiliang University, Hangzhou 310018, P.R. China*

Yadong Sun − *Department of Physics, China Jiliang University, Hangzhou 310018, P.R. China*

Complete contact information is available at: https://pubs.acs.org/10.1021/acs.langmuir.3c02655

Author Contributions

‖S.Y. and J.Z. contributed equally to this paper.

Notes

The authors declare no competing financial interest.

ACKNOWLEDGMENTS

This work was supported by the National Natural Science Foundation of China (Nos. 12172113, 12025206), the Natural Science Foundation of Zhejiang Province (No. LZ23A020003), and the National Key Research and Development Program of China (No. 2022YFA1203602).

REFERENCES

(1) Bowden, N.; Brittain, S.; Evans, A. G.; Hutchinson, J. W.; Whitesides, G. M. Spontaneous Formation of Ordered Structures in Thin Films of Metals Supported on an Elastomeric Polymer. *Nature* **1998**, *393*, 146−149.

(2) Cai, S.; Breid, D.; Crosby, A. J.; Suo, Z.; Hutchinson, J. W. Periodic Patterns and Energy States of Buckled Films on Compliant Substrates. *J. Mech. Phys. Solids* **2011**, *59*, 1094−1114.

(3) Cerda, E.; Mahadevan, L. Geometry and Physics of Wrinkling. *Phys. Rev. Lett.* **2003**, *90*, No. 074302.

(4) Yin, J.; Yagüe, J. L.; Eggenspieler, D.; Gleason, K. K.; Boyce, M. C. Deterministic Order in Surface Micro-Topologies through Sequential Wrinkling. *Adv. Mater.* **2012**, *24*, 5441−5446.

(5) Hwang, M.; Kim, C.; Kim, J.; Son, J. G.; Yeom, B. Controlled Fabrication of 3D Chiral Microwrinkles via Asymmetrical and Biaxial Bucklings. *Adv. Funct. Mater.* **2019**, *29*, No. 1808979.
(6) Pellegrino, L.; Tan, A.; Cabral, J. T. Ripple Patterns Spontaneously Emerge through Sequential Wrinkling Interference in Polymer Bilayers. *Phys. Rev. Lett.* **2022**, *128*, No. 058001.
(7) Xue, Z.; Song, H.; Rogers, J. A.; Zhang, Y.; Huang, Y. Mechanically-Guided Structural Designs in Stretchable Inorganic Electronics. *Adv. Mater.* **2020**, *32*, No. 1902254.
(8) Ma, L.; He, L.; Ni, Y. Tunable Hierarchical Wrinkling: From Models to Applications. *J. Appl. Phys.* **2020**, *127*, No. 111101.
(9) Lee, G.; Zarei, M.; Wei, Q.; Zhu, Y.; Lee, S. G. Surface Wrinkling for Flexible and Stretchable Sensors. *Small* **2022**, *18*, No. 2203491.
(10) Yuan, L.; Chen, J.; Li, Y.; Luo, G.; Gao, Z.; Zhou, C.; Li, H.; Xu, P.; Zong, C. Flexible Azo-Polyimide-Based Smart Surface with Photoregulatable Surface Micropatterns: Toward Rewritable Information Storage and Wrinkle-Free Device Fabrication. *Langmuir* **2023**, *39*, 2787−2796.
(11) Chen, D.; McKinley, G. H.; Cohen, R. E. Spontaneous Wettability Patterning via Creasing Instability. *Proc. Natl. Acad. Sci. U. S. A.* **2016**, *113*, 8087−8092.
(12) Nagashima, S.; Nakatani, A. Capillary-Induced Wrinkle-to-Fold Transitions under Biaxial Compression. *Langmuir* **2021**, *37*, 5282−5289.
(13) Brau, F.; Vandeparre, H.; Sabbah, A.; Poulard, C.; Boudaoud, A.; Damman, P. Multiple-Length-Scale Elastic Instability Mimics Parametric Resonance of Nonlinear Oscillators. *Nat. Phys.* **2011**, *7*, 56−60.
(14) Zang, J.; Zhao, X.; Cao, Y.; Hutchinson, J. W. Localized Ridge Wrinkling of Stiff Films on Compliant Substrates. *J. Mech. Phys. Solids* **2012**, *60*, 1265−1279.
(15) Wang, Q.; Zhao, X. A Three-Dimensional Phase Diagram of Growth-Induced Surface Instabilities. *Sci. Rep.* **2015**, *5*, No. 8887.
(16) Wang, Q.; Zhao, X. Beyond Wrinkles: Multimodal Surface Instabilities for Multifunctional Patterning. *MRS Bull.* **2016**, *41*, 115−122.
(17) Cao, C.; Chan, H. F.; Zang, J.; Leong, K. W.; Zhao, X. Harnessing Localized Ridges for High-Aspect-Ratio Hierarchical Patterns with Dynamic Tunability and Multifunctionality. *Adv. Mater.* **2014**, *26*, 1763−1770.
(18) Takei, A.; Jin, L.; Hutchinson, J. W.; Fujita, H. Ridge Localizations and Networks in Thin Films Compressed by the Incremental Release of a Large Equi-Biaxial Pre-Stretch in the Substrate. *Adv. Mater.* **2014**, *26*, 4061−4067.
(19) Jin, L.; Takei, A.; Hutchinson, J. W. Mechanics of Wrinkle/Ridge Transitions in Thin Film/Substrate Systems. *J. Mech. Phys. Solids* **2015**, *81*, 22−40.
(20) Auguste, A.; Yang, J.; Jin, L.; Chen, D.; Suo, Z.; Hayward, R. C. Formation of High Aspect Ratio Wrinkles and Ridges on Elastic Bilayers with Small Thickness Contrast. *Soft Matter* **2018**, *14*, 8545−8551.
(21) Guan, X.; Sarma, A. P.; Hamesh, E. K.; Yang, J.; Nguyen, N.; Cerda, E.; Pocivavsek, L.; Velankar, S. S. Compression-Induced Buckling of Thin Films Bonded to Viscous Substrates: Uniform Wrinkles vs Localized Ridges. *Int. J. Solids Struct.* **2022**, *254*, No. 111843.
(22) Ebata, Y.; Croll, A. B.; Crosby, A. J. Wrinkling and Strain Localizations in Polymer Thin Films. *Soft Matter* **2012**, *8*, 9086−9091.
(23) Lu, C.; Yu, S.; Li, H.; Zhou, H.; Jiao, Z.; Li, L. Harnessing Heterogeneous Wrinkles in Metal/Polydimethylsiloxane Film System by Combination of Mechanical Loading and Heat Treatment. *Adv. Mater. Interfaces* **2020**, *7*, No. 1902188.
(24) Takei, A.; Jin, L.; Fujita, H.; Jin, L. High-Aspect-Ratio Ridge Structures Induced by Plastic Deformation as a Novel Microfabrication Technique. *ACS Appl. Mater. Interfaces* **2016**, *8*, 24230−24237.
(25) Khang, D. Y.; Jiang, H.; Huang, Y.; Rogers, J. A. A Stretchable Form of Single-Crystal Silicon for High-Performance Electronics on Rubber Substrates. *Science* **2006**, *311*, 208−212.
(26) Lin, C. B.; Chuang, Y. F.; Yang, F.; Lee, S. Kinetics for the Slip Motion of Ripple Dislocations on Gold-Coated Poly (dimethylsiloxane). *Langmuir* **2021**, *37*, 5943−5949.
(27) Knapp, A.; Nebel, L. J.; Nitschke, M.; Sander, O.; Fery, A. Controlling Line Defects in Wrinkling: A Pathway Towards Hierarchical Wrinkling Structures. *Soft Matter* **2021**, *17*, 5384−5392.
(28) Yu, S.; Liu, X.; Sun, Y.; Zhou, H.; Cai, P. Formation, Evolution and Transition of Multiple Surface Patterns in Metal Films on Polymer Substrates under Uniaxial Loading. *Thin Solid Films* **2019**, *669*, 355−363.
(29) Li, Z.; Zhai, Y.; Wang, Y.; Wendland, G. M.; Yin, X.; Xiao, J. Harnessing Surface Wrinkling-Cracking Patterns for Tunable Optical Transmittance. *Adv. Opt. Mater.* **2017**, *5*, No. 1700425.
(30) Yu, S.; Ma, L.; He, L.; Ni, Y. Hierarchical Crack Patterns of Metal Films Sputter Deposited on Soft Elastic Substrates. *Phys. Rev. E* **2019**, *100*, No. 052804.
(31) Liu, M.; Yu, S.; He, L.; Ni, Y. Recent Progress on Crack Pattern Formation in Thin Films. *Soft Matter* **2022**, *18*, 5906−5927.
(32) Ni, Y.; Yu, S.; Jiang, H.; He, L. The Shape of Telephone Cord Blisters. *Nat. Commun.* **2017**, *8*, No. 14138.
(33) Wang, E.; Xiong, Z.; Chen, Z.; Xin, Z.; Ma, H.; Ren, H.; Wang, B.; Guo, J.; Sun, Y.; Wang, X.; Li, C.; Li, X.; Liu, K. Water Nanolayer Facilitated Solitary-Wave-Like Blisters in MoS_2 Thin Films. *Nat. Commun.* **2023**, *14*, 4324.
(34) Nolte, A. J.; Chung, J. Y.; Davis, C. S.; Stafford, C. M. Wrinkling-to-Delamination Transition in Thin Polymer Films on Compliant Substrates. *Soft Matter* **2017**, *13*, 7930−7937.
(35) Pan, K.; Ni, Y.; He, L.; Huang, R. Nonlinear Analysis of Compressed Elastic Thin Films on Elastic Substrates: from Wrinkling to Buckle-Delamination. *Int. J. Solids Struct.* **2014**, *51*, 3715−3726.
(36) Yu, S.; Zhang, J.; Li, H.; Li, L.; Ni, Y. Controllable Buckle Delaminations in Polymer-Supported Periodic Gradient Films by Mechanical Compression. *Langmuir* **2022**, *38*, 13469−13476.
(37) Pocivavsek, L.; Dellsy, R.; Kern, A.; Johnson, S.; Lin, B.; Lee, K. Y. C.; Cerda, E. Stress and Fold Localization in Thin Elastic Membranes. *Science* **2008**, *320*, 912−916.
(38) Chen, Y. C.; Crosby, A. J. Wrinkling of Inhomogeneously Strained Thin Polymer Films. *Soft Matter* **2013**, *9*, 43−47.
(39) Chen, Y. C.; Crosby, A. J. High Aspect Ratio Wrinkles via Substrate Prestretch. *Adv. Mater.* **2014**, *26*, 5626−5631.
(40) Cheng, Z.; Xu, F. Intricate Evolutions of Multiple-Period Post-Buckling Patterns in Bilayers. *Sci. China Phys. Mech.* **2021**, *64*, No. 214611.
(41) Fu, C.; Cheng, Z.; Wang, T.; Xu, F. An Asymptotic Modeling and Resolution Framework for Morphology Evolutions of Multiple-Period Post-Buckling Modes in Bilayers. *Math. Mech. Solids* **2022**, *27*, 1397−1411.
(42) Cao, Y.; Hutchinson, J. W. Wrinkling Phenomena in Neo-Hookean Film/Substrate Bilayers. *J. Appl. Mech.* **2012**, *79*, No. 031019.
(43) Jiang, H.; Khang, D. Y.; Song, J.; Sun, Y.; Huang, Y.; Rogers, J. A. Finite Deformation Mechanics in Buckled Thin Films on Compliant Supports. *Proc. Natl. Acad. Sci. U.S.A.* **2007**, *104*, 15607−15612.

https://doi.org/10.1021/acs.langmuir.3c02655
Langmuir 2024, 40, 403−412